Research article **Open Access**

Pedram Sadeghi, Kaiyu Wu, Tomas Rindzevicius, Anja Boisen and Silvan Schmid*

Fabrication and characterization of Au dimer antennas on glass pillars with enhanced plasmonic response

DOI 10.1515/nanoph-2017-0011
Received January 18, 2017; revised April 4, 2017; accepted April 7, 2017

Abstract: We report on the fabrication and dark-field spectroscopy characterization of Au dimer nanoantennas placed on top of SiO_2 nanopillars. The reported process enables the fabrication of nanopillar dimers with gaps down to 15 nm and heights up to 1 μm. A clear dependence of the plasmonic resonance position on the dimer gap is observed for smaller pillar heights, showing the high uniformity and reproducibility of the process. It is shown how increasing the height of nanopillars significantly affects the recorded elastic scattering spectra from Au nanoantennas. The results are compared to finite-difference time-domain (FDTD) and finite-element method (FEM) simulations. Additionally, measured spectra are accompanied by dark-field microscopy images of the dimers, showing the pronounced change in color. Placing nanoantennas on nanopillars with a height comparable to the in-plane dimer dimensions results in an enhancement of the scattering response, which can be understood through reduced interaction of the near-fields with the substrate. When increasing the pillar height further, scattering by the pillars themselves manifests itself as a strong tail at lower wavelengths. Additionally, strong directional scattering is expected as a result of the interface between the nanoantennas and nanopillars, which is taken into account in simulations. For pillars of height close to the plasmonic resonance wavelength, the scattering spectra become more complex due to additional scattering peaks as a result of larger geometrical nonuniformities.

***Corresponding author: Silvan Schmid,** TU Wien, Institute of Sensor and Actuator Systems, Gusshausstrasse 27–29, 1040 Wien, Austria, e-mail: silvan.schmid@tuwien.ac.at. http://0000-0001-9508-2034
Pedram Sadeghi: TU Wien, Institute of Sensor and Actuator Systems, Gusshausstrasse 27–29, 1040 Wien, Austria
Kaiyu Wu, Tomas Rindzevicius and Anja Boisen: DTU Nanotech, Institute for Micro- and Nanotechnology, Oersteds Plads, 2800 Kgs. Lyngby, Denmark

Keywords: gap plasmons; enhanced plasmon resonance; plasmonic sensing; surface-enhanced Raman spectroscopy; nonlinear response.

1 Introduction

Localized surface plasmon resonance (LSPR) in strongly coupled subwavelength metal nanoparticles has received a tremendous amount of interest in recent years, due to the ability to confine and enhance electromagnetic fields in nanometer-sized regions [1]. The LSPRs associated with such structures display a huge dependence on the particle shape, size, interparticle separation and dielectric environment, enabling such structures to be used, e.g. for biosensing, where minute concentrations of analyte molecules can induce changes in the LSPR peak position [2–4]. Other applications include surface-enhanced Raman spectroscopy (SERS) [5], surface-enhanced infrared absorption (SEIRA) [6], photodetectors [7] and nonlinear optics [8]. One challenge for actual practical applications of LSPRs has been the deterioration of the plasmonic response as a result of the particles being placed on a substrate [9]. Indeed, studies have shown that the presence of a substrate negatively affects the near-field enhancement, extinction cross-section, and refractive index sensitivity of nanoantennas, as well as shifting the resonance away from theoretically expected values [10–12].

One method for overcoming the limitations set by the substrate is to place the nanoparticles on nanopedestals or nanopillars [13]. The lifting of the nanoantennas results in reduced overlap of the electromagnetic fields with the substrate, thus increasing the overall field enhancement and, as a result, also the refractive index sensitivity, in addition to boosting the SERS and SEIRA signal [14–17]. Elevation is typically achieved by either wet etching or reactive-ion etching (RIE) of the substrate, while the nanoantennas serve as an etch mask [18]. As a result, structures can be fabricated on various substrates,

depending on the application and desired resonance wavelength. Furthermore, the size, shape, and distribution of the particles can be precisely defined, only limited by the resolution of typically employed fabrication methods, such as, e.g. electron beam lithography (EBL) [19, 20]. Alternatively, deposition of metal can be done post-etching, forming a cavity between the nanoantennas and the underlying substrate [21, 22]. These studies show the promise of using nanopillars for future plasmonic applications.

Thus far, most experimental studies have focused on long-range ordered arrays of nanoantennas with grating constants on the order of the visible light wavelength [23]. For the purpose of large-area sensing and commercial devices, having many sensors per cm^2 is beneficial in terms of boosting the signal. Furthermore, when the periodicity of dimers matches the LSPR wavelength or the probe laser wavelength, even larger field enhancements and SERS signals have been observed, respectively [15, 24]. However, in order to understand how nanopillars themselves affect the plasmonic response, it is important to study isolated nanoantennas, i.e. with separations between nanoantennas significantly larger than the LSPR wavelength. In this regime, any diffractive coupling between the antennas can be neglected and thus, the spectra should be readily comparable to numerical simulations [25, 26].

Here, we present the fabrication and dark-field scattering characterization of individual Au dimers on nanopillars etched directly out of commercial fused silica substrates. Using the presented fabrication process, nanopillar dimers can be fabricated with interparticle gaps down to 15 nm. Importantly, the aspect ratio of the pillars can reach up to around 8, reaching a regime that is not discussed a lot in literature. We study the dark-field scattering signal from individual dimers and compare the results to finite-difference time-domain (FDTD) simulations. A clear enhancement of the scattering response is observed when placing the nanoantennas on 240 nm tall pillars, which can be explained through reduced screening of the near-fields by the substrate. As the height of the pillars is increased further, pronounced changes in the scattering response are observed. For pillars of 480 nm height, scattering by the pillars themselves starts to play an important role in the measured spectra, manifesting itself as a strong tail at lower wavelengths. Furthermore, an additional mode at a wavelength of 540 nm is observed. The peculiar scattering spectrum is believed to arise due to the angled incidence of the white light and large-angle scattering due to the nanoantenna/nanopillar interface. As a result, only forward scattered light is taken into account in the simulations at these pillar heights. Dimers on 740 nm tall pillars display multiple resonances in the visible to near-infrared spectral range. We interpret this as a result of varying antenna gaps due to pillar leaning.

All structures were fabricated with a varying antenna gap in order to further characterize the modes and show that the fabrication process leaves the antennas unharmed. As the antenna gap is varied, the LSPR shifts are in agreement with simulations for the 240 nm pillars, showing that the process is reliable and reproducible for shorter pillar heights.

2 Materials and methods

2.1 Sample fabrication

Nanopillar dimer arrays are fabricated using a combination of EBL and RIE, similar to previous reports on bowtie nanopillar dimer fabrication [27]. An overall schematic of each step in the process is given in Figure 1A. An approximately 140 nm thick layer of SX AR-P 6200/2 (CSAR resist, AR-600-546, and AR-600-71, ALLRESIST GmbH, Am Biotop, Strausberg, Germany) is spun onto a commercial 500 μm thick 4-inch fused silica wafers (Innergie Technologies Inc., Gonjiam-Eup, Gwangju-Si, Gyeonggi-Do, South Korea) at 6000 rpm for 60 s, followed by a 5 min softbake at 180°C. In order to avoid charging during EBL steps, a 15 nm Al layer is deposited using thermal evaporation. Arrays of round nanoparticle dimers are then patterned using EBL (JEOL JBX-9500FS, JEOL USA, Inc., Peabody, MA, USA) at 100 kV accelerating voltage, 300 $\mu C/cm^2$ dosage, and 0.8 nA beam current. Nanoparticle diameters of 120 nm and 150 nm were designed, with variable interparticle gaps of 15–30 nm. After exposure, the Al layer is removed in a solution of Microposit MF-322 Developer (Shipley Company, Marlborough, MA, USA) for 50 s. Developing of the resist is done using AR-600-546 for 60 s at room temperature.

Using electron beam evaporation (Physimeca ΦSES250, Physimeca Technologie, Villiers le Bacle, France), 2 nm Cr, 40 nm Au, and 30 nm Ni are deposited, with the Ni layer serving as a protecting layer for the Au in the RIE step. Lift-off of excess resist/metal is done using Remover AR-600-71. Nanopillars are then defined using RIE (STS Cluster System C010, SPTS Technologies Ltd., Newport, UK) using 60 sccm CF_4 at a power and pressure of 30 W and 60 mTorr, respectively. For the 480 nm tall pillars discussed below, a recipe consisting of 14 sccm

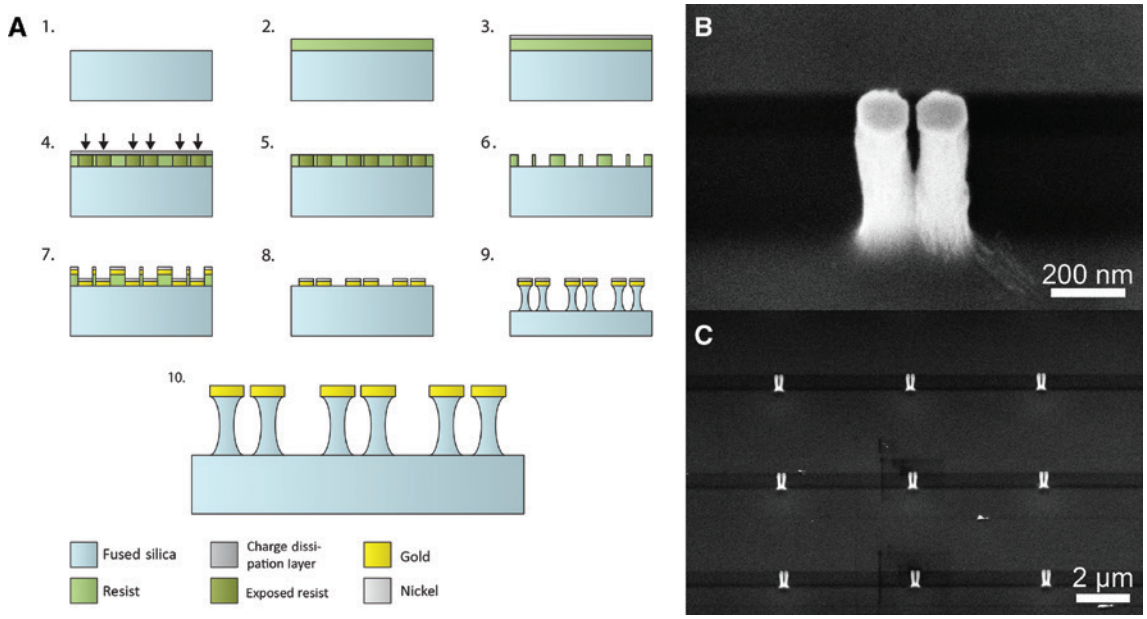

Figure 1: Fabrication of nanopillar dimer arrays.
(A) Schematic of the individual process steps to fabricate nanopillar dimer arrays, involving electron-beam lithography to define nanodisk dimers and reactive-ion etching of the substrate to form nanopillars. (B) Scanning electron micrograph of a single 150 nm diameter 400 nm tall nanopillar dimer with a gap of 15 nm. (c) Array of 5 µm separated nanopillar dimers with a pillar height of 740 nm.

CHF_3 and 26 sccm CF_4 was used, with a power and pressure set to 60 W and 100 mTorr, respectively. After RIE, the remaining Ni is removed using a 17% HNO_3 solution, leaving the Au and pillars unchanged.

Figure 1B shows a scanning electron microscopy image of a single 150 nm diameter nanopillar dimer with a pillar height of 400 nm. The nanoantenna gap is around 15 nm, the highest resolution achieved with the process. A high uniformity is achieved, as evident from Figure 1C, which shows an array of 740 nm tall nanopillar dimers with a grating constant of 5 µm.

2.2 Dark-field measurement setup

Optical scattering spectra of nanopillar dimers are measured using a dark-field microscope (Nikon, Ti-U, Nikon Corporation, Shinagawa, Tokyo, Japan). White light from a halogen lamp is shone through a dark-field condenser (NA = 0.8–0.95) onto the sample with the pillars placed face up. A linear polarizer is placed prior to the condenser in order to control the polarization of the incoming light, and an aluminum blocker is used to filter out light at perpendicular angles. Forward scattered light is collected by a 60× objective (Nikon Corporation, Shinagawa, Tokyo, Japan, air immersion, NA = 0.7) and sent to a spectrometer (Andor SR-303i, Andor Technology Ltd., Belfast, UK) equipped with an electron multiplying charge-coupled device (EMCCD) (Andor Newton, Andor Technology Ltd., Belfast, UK) detector [28]. Scattering spectra are measured over the wavelength range of 400–1000 nm. For dark-field imaging of the structures, the light is guided to a complementary metal-oxide-semiconductor (CMOS Camera, EO-18112, Edmund Optics Inc., Barrington, NJ, USA). A schematic of the setup is given in Figure 2A.

The final spectra are extracted by subtracting a background from a dark area on the sample and then dividing by the spectrum of the halogen lamp [29]. All spectra presented here are averages of a line of 10 dimers separated by 5 µm, large enough to avoid diffractive coupling between different dimers. A small enough number of dimers are used so that only minimal broadening of the response as a result of inhomogeneity is expected, while increasing the measured signal. For the following discussion, all shown spectra are acquired with the polarization of the incident light parallel to the dimer axis.

2.3 Numerical simulations

Scattering spectra and electromagnetic field distributions were mainly simulated based on the FDTD method (Lumerical Solutions). Nanoantennas and nanopillars are

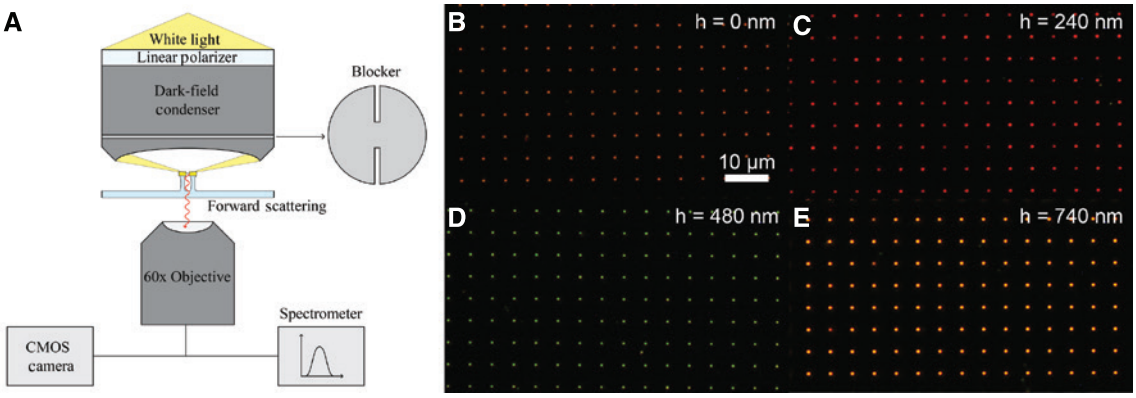

Figure 2: Optical dark-field setup employed to measure scattering of nanopillar dimers.
(A) Schematic of the individual elements of the setup. Forward scattered light is sent either to a CMOS camera for imaging or a spectrometer for scattering analysis. (B)–(E) Dark-field images of nanoantenna dimers without pillars and with 240 nm, 480 nm, and 740 nm tall pillars. A clear change in color can be observed with increasing height.

defined as cylinders of equal diameter. In order to mimic experimental situations, the nanopillars are placed on an SiO_2 substrate with dimensions large enough to be considered "infinite". The thickness of the nanoantennas is kept fixed at 40 nm, while the real and imaginary parts of the Au dielectric function are obtained from experimental data by Johnson and Christy [30]. For the SiO_2 nanopillars and substrate, data from Palik [31] are used for the dielectric function, while the surrounding medium index is set to $n_m = 1$. Due to the structure of the simulation, symmetry could be applied to the x and y boundaries in order to decrease simulation time. Perfectly matched layers (PMLs) were used on the remaining boundaries. The simulation region is made significantly larger than the nanopillar dimer structure in order to avoid the evanescent tails of the plasmon resonance interacting with the PML boundaries. Structures are illuminated with a plane wave from the nanoantenna side at normal incidence, while the polarization is set parallel to the dimer axis. For the nanoantennas and nanopillars, a mesh size of $1 \times 1 \times 1$ nm^3 is used, while the remaining structure is defined by the built-in nonuniform mesh algorithm of the software with a mesh accuracy of 4. All simulated scattering cross-sections are normalized to the geometrical cross-section of the dimers and this is therefore termed scattering efficiency in the following sections.

More advanced simulations were performed using the finite-element method (FEM, Comsol Multiphysics). The simulation setup is similar to the FDTD simulations, Lumerical Solutions, Inc., Vancouver, BC, Canada, also using PMLs to minimize nonphysical reflections at the boundaries. However, a highly non-uniform adaptive mesh is employed to increase the accuracy of the calculation.

3 Results and discussion

3.1 Nanopillar-induced change of the plasmonic response

The influence of the nanopillar height on the plasmonic response is studied for 150 nm diameter nanoantenna dimers with a nominal gap of 30 nm. Figure 2B–E show dark-field microscopy images of arrays of such dimers placed on pillars of 0 nm, 240 nm, 480 nm, and 740 nm height, respectively. From the dark-field images, it is evident that pillar height strongly influences the optical response, displayed by the height-dependent coloring of the dimers. Evidently, pillar height not only enhances the plasmonic response, but significantly alters the observed spectral signatures. In order to understand the difference in colors, each case will subsequently be studied in more detail.

Figure 3A shows the measured pillar height-dependent scattering response of the nanoantenna dimers. The respective (FEM simulation, COMSOL, Inc., Burlington, MA, USA) spectra are displayed in Figure 3B. FDTD was not used in this case due to the simplicity of the simulation geometry, as discussed further below. For the case without pillars, a single broad peak is observed at $\lambda = 780$ nm, which is the expected gap-dependent plasmonic mode. Putting the nanoantenna on top of 240 nm nanopillars results in a significant expected enhancement of the scattering amplitude. Furthermore, the peak is narrowed, which is important for LSPR based sensing applications. The measured spectra are in good agreement with the simulations. The small discrepancies regarding the exact peak position can be attributed to pillar imperfections of the nanofabricated samples. In particular, smaller

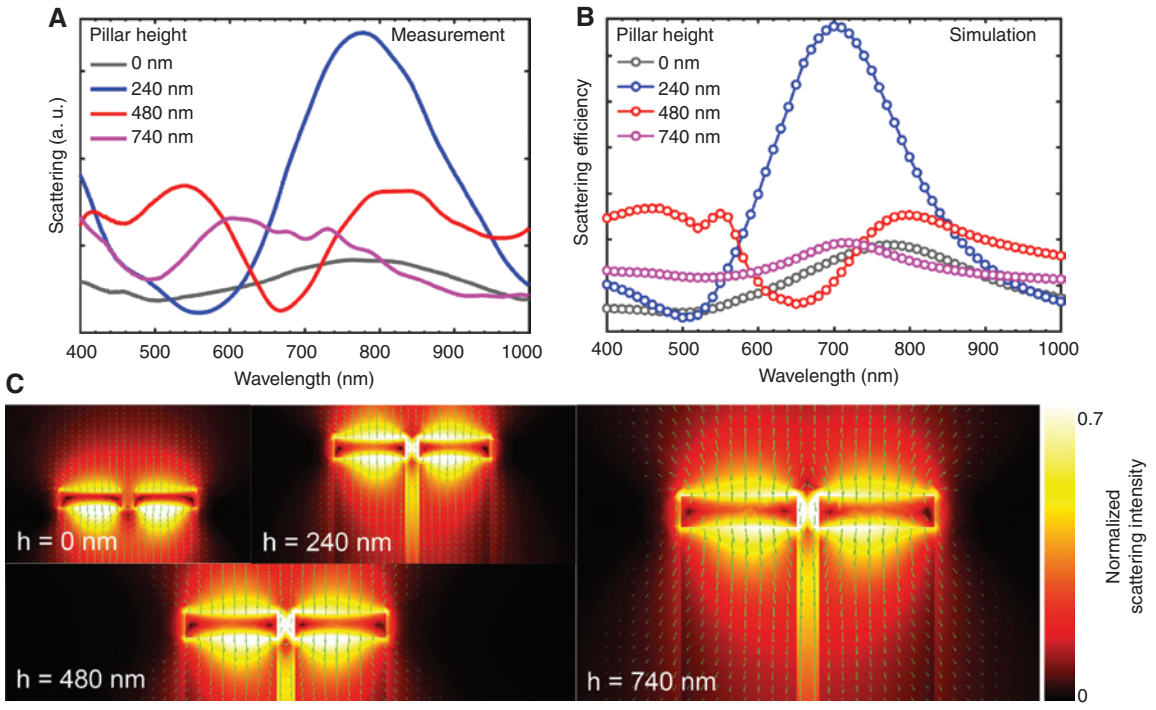

Figure 3: Scattering spectra of 150 nm diameter nanoantenna dimers with a gap of 30 nm on top of nanopillars of various height. (A) Comparison between measured scattering spectra of 0 nm, 240 nm, 480 nm, and 740 nm tall nanopillar dimers. A clear enhancement is observed when placing the antennas on 240 nm tall pillars, but the degree of enhancement decreases for taller heights, which is due to a significant portion of the light being scattered at larger angles than the forward direction. (B) Corresponding simulated spectra of the data shown in (A). By only taking forward scattered light into consideration and coming with an angle equal to that of the dark-field condenser, the simulated spectra show reasonable agreement with experimental spectra. (C) Plots of the intensity and power flow of the scattering of a nanoantenna dimer for various pillar heights at an excitation wavelength of 800 nm, plotted in the center transverse plane of the structures. A portion of the light is scattered at larger angles due to the interface between gold and glass, which will alter the forward scattered spectrum.

inter-dimer gaps could be causing the observed overall redshifting of the peaks.

The associated dark-field images presented in Figure 2B and C for dimers without and with 240 nm pillars, respectively, support the observed spectra. The dim red color of the pillarless dimers becomes a bright red for the pillar-enhanced dimers. On closer inspection of the dark-field images, slight differences in brightness and color can be observed in the array of pillar dimers, due to variations of the gap distance. The dark-field images can be readily used to characterize the homogeneity of plasmonic structures. For example for thinner pillars with a diameter of 120 nm, clear color changes of individual nanoantennas that are leaning against each other can be observed (see Supplementary Information).

As mentioned above, tall pillars are flexible enough to create a leaning effect, closing the antenna gap to sub-nm dimensions, which is ideal for, e.g. SERS [32, 33]. As a result, nanopillar arrays were fabricated with taller pillar heights up to ≈1 µm. Only the case of 480 nm and 740 nm pillar heights are shown here. Pillars taller than 740 nm became too flexible and all started to lean. The resulting undefined dimer gap distances makes a meaningful study of such pillars difficult.

The measured scattering spectrum of 480 nm tall nanopillar dimers, in addition to the expected plasmon resonance around $\lambda = 820$ nm, shows another peak at $\lambda = 540$ nm. This additional peak is responsible for the dimers' green color in the respective dark-field image (Figure 2D), since the actual plasmon mode is located in the, for the eye, invisible near-infrared. The dimers appear very uniform in terms of color and brightness, compared to the case of 240 nm tall pillars. This suggests that the lower resonance is independent of dimer gap size, which typically shows slight fabrication induced variations. The pillar height, by contrast, is defined by the etching time, and typically shows good homogeneity. Hence, the peak at $\lambda = 540$ nm could be caused by a cavity resonance between the Au dimers and the glass substrate.

FDTD simulations of the scattering response were not in agreement with the observed spectra (not shown here). The reason is the difference in experimental and simulation conditions. For the experiments, the incoming light arrives at an angle and only forward scattered light is

collected, while for the simulations, the excitation light is perpendicular to the dimer plane and light scattered at all angles is collected for the final spectrum. Nanoantennas close to an interface, such as an underlying substrate, have been shown to scatter at angles larger than the critical angle for the interface [34]. Thus, using air objectives, a large portion of the scattered light will not reach the detector. Suspending the nanoantennas above nanopillars changes the amount of light in the forward direction, additionally altering the measured spectra.

Due to the oversimplified geometry in the normal scattering simulations discussed above, the simulation geometry is altered to match experimental conditions. These simulations were done using FEM. Light arrives at an angle of 72° and only forward scattered light is used for the final spectrum. As a result, much better agreement between simulations and experiments is achieved. Figure 3C shows plots of the scattering intensity and scattering power flow for all cases studied here at an excitation wavelength of 800 nm, plotted in the center transverse plane of the structures. As expected, a portion of the light can be seen to scatter at large angles, thus not reaching the detector in the measurements and altering the spectra.

The additional features in the spectrum for the 480 nm tall nanopillars can be attributed to an interference effect at the pillar/substrate interface for this specific height, as the other heights only display a single scattering peak, as mentioned above. The overall lower scattering amplitude with increasing pillar height is attributed to a smaller portion of the light reaching the detector for the taller pillars due to large-angle scattering.

Finally, for a height of 740 nm, the spectrum displays a number of different peaks in the wavelength range of $\lambda \approx 500–900$ nm. The overall scattering amplitude has also decreased even further. A corresponding dark-field image of a 740 nm tall pillar array is shown in Figure 2E. The pillars appear slightly orange in color, which is due to the mode at $\lambda \approx 600$ nm having the largest scattering amplitude. FEM simulations show a peak at $\lambda = 715$ nm, but do not display the additional features measured experimentally. This could be a result of a higher degree of nonuniformity for such tall pillars, so that the overall scattering spectrum becomes an average of 10 slightly different dimers.

All measured spectra in Figure 3A show a scattering increase at wavelengths below 500 nm. Apparently, the tail at lower wavelengths is smallest in amplitude in the case of nanoantennas without pillars. This would suggest that the pillars themselves are responsible for the additional scattering. To back up the proposed hypothesis, FDTD simulations were done without any Au on the pillars, in order to get the scattering response of the pillars alone. Figure 4A shows the simulated scattering spectra of a bare 150 nm diameter SiO_2 nanopillar dimer for heights of 240 nm, 480 nm, and 740 nm, compared to the case of a SiO_2 substrate alone. The tail is clearly present and increases in amplitude with increasing pillar height, confirming that the pillars themselves are responsible for the additional scattering. Further confirmation is achieved by plotting the spectrum of a 480 nm tall pillar dimer with and without dimer antennas on top, as shown in Figure 4B. A steady increase in the tail amplitude with increasing height is not observed experimentally or in the FEM simulations, which can be attributed to the pillars not necessarily scattering in the forward direction.

3.2 Gap-dependence of the plasmonic modes

In order to show that the fabrication process allows the creation of nanoantennas with defined dimer gaps, we

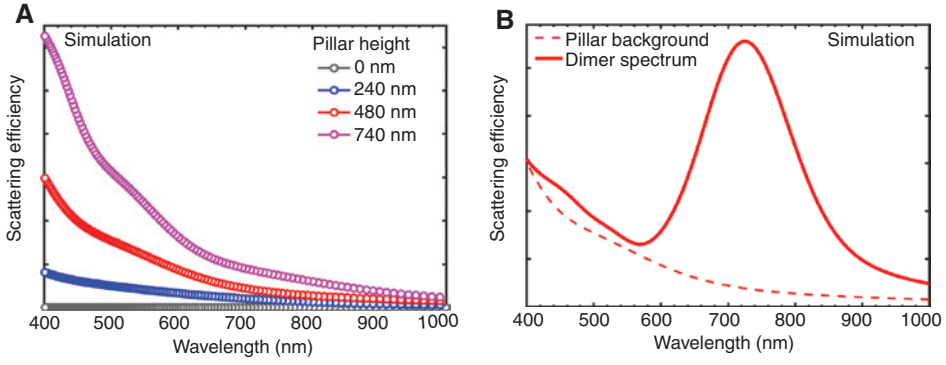

Figure 4: Effect of nanopillar height on scattering spectra.
(A) Simulated scattering spectra of 150 nm diameter nanopillar dimers with a 30 nm gap without Au nanoantennas on top. A tail clearly forms at lower wavelengths, which increases with increasing pillar height. (B) Plot of the 480 nm diameter spectrum with and without nanoantennas, showing that the tail is present in both cases.

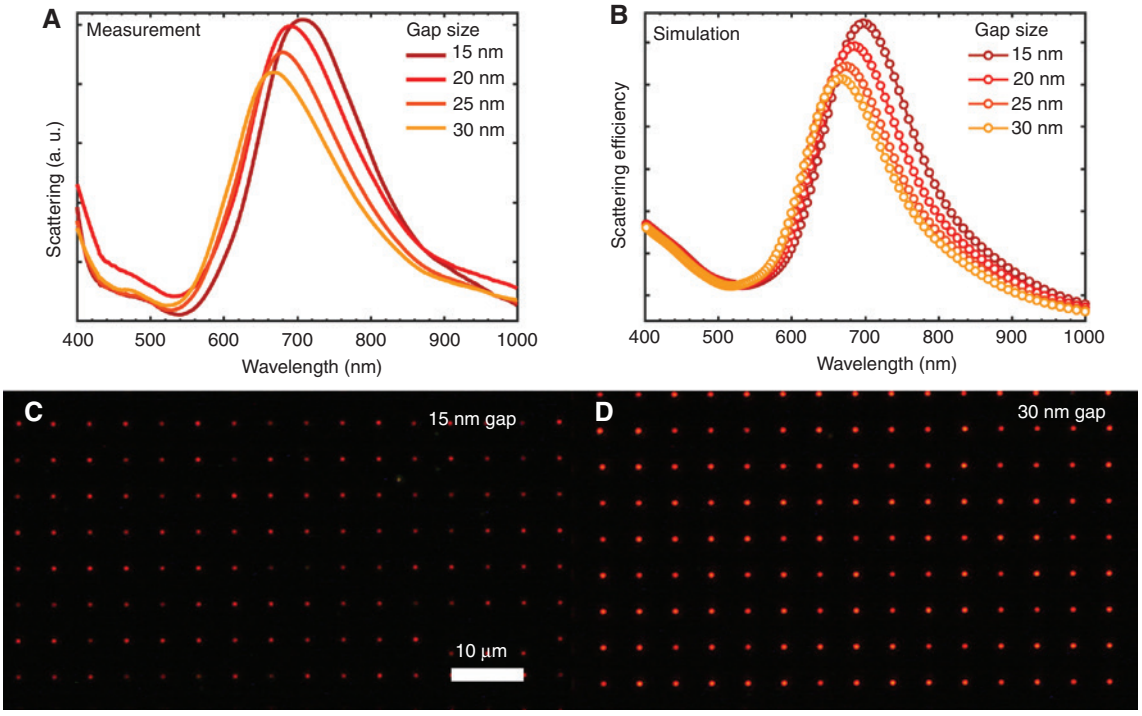

Figure 5: Gap-dependence of the plasmonic resonance for 120 nm diameter nanoantennas on 240 nm tall nanopillars. (A) Measured scattering spectra, displaying a clear blueshifting of the resonance with increasing gap. (B) Simulation of the spectra shown in (A). The large agreement shows the uniformity and precise gap definition of the samples. (C) Dark-field images of an array with 15 nm gap, where the slight differences in color can be observed due to the small gap being close to the limit of EBL. (D) Same as in (C) for a gap of 30 nm, showing a much larger uniformity due to the larger gap size.

have fabricated dimers with gaps from 15 nm to 30 nm and studied the scattering response for each gap. This is of particular importance to LSPR sensing and SERS applications. Figure 5A shows the measured scattering spectra for 120 nm diameter nanoantennas on 240 nm tall nanopillars for various gap sizes. A clear red-shifting of the LSP resonance is observed with decreasing gap, in agreement with FDTD simulations shown in Figure 5B. This shows that the nanoantennas have gaps with good uniformity.

The effect of the gap distance on the plasmonic response can be readily observed via the color change in respective dark-field microscopy images. Figure 5C and D show an array of 120 nm diameter dimers, with gaps of 15 nm and 30 nm, respectively. For the 15 nm separated dimers, the color appears dim and nonuniform, possibly due to the gap size being at the limit of EBL for such a thick resist. As such, a higher degree of variation in gap should be expected. Furthermore, at such small gaps, the resonance position is very sensitive to the exact gap size and shape. However, for the 30 nm separated dimers, the color appears bright red and uniform, since the gap size is well within the reach of EBL. The color is also lighter red, directly showing the blue-shift in the LSP resonance wavelength.

4 Conclusion

We have fabricated arrays of Au nanopillar dimers with well-defined heights and gaps by RIE using commercial fused silica substrates. By making the array pitch significantly larger (5 µm) than the dimer resonance wavelength, we were able to study the elastic scattering response of individual Au pillar dimers and investigate what impact pillar height has on the plasmonic properties of the dimers. Importantly, it was found that the interface between the nanoparticles and nanopillars results in significant large-angle scattering, which affects the measured spectra due to collecting only forward scattered light. As a result, FEM simulations were done with the simulation geometry adjusted to match the experimental conditions in order to properly reproduce the measured spectra. Placing the nanoantennas on 240 nm tall nanopillars resulted in a huge enhancement of the scattering response in terms of both peak amplitude and linewidth. Doubling the pillar height to 480 nm results in pronounced changes at lower wavelengths in the shape of an additional peak and a tail in scattering, with the former possibly being a pillar-induced plasmonic

mode, while the latter is a result of scattering by the pillars themselves. Simulations without antennas further confirms that the pillars create additional scattering at lower wavelengths, which can potentially dominate the spectrum at very tall pillar heights. Finally, pillars with heights of 740 nm display multiple resonances in the $\lambda \approx 500–900$ nm range, making it difficult to characterize the fundamental gap-dependent mode of the pillars. Simulations only display a single peak, meaning that the multiple resonances are most likely due to a lack of uniformity for different dimers. These findings show both the promise and limitations of nanopillar based plasmonic sensors and that increasing height adds additional complexity to the elastic scattering spectra, which needs to be taken into account.

Measured spectra are supported by dark-field microscopy images of the arrays. From imaging alone, clear changes in the color can be observed with increasing pillar height, while minor differences in color in individual samples can be used to investigate uniformity. As such, dark-field imaging proves to be a powerful tool for characterizing plasmonic samples without the need for data extraction and manipulation.

Acknowledgments: P.S. and S.S. would like to acknowledge financial support from the ERC grant PLASMECS and the Villum Foundations Young Investigator Programme (Project No. VKR023125). T.R. and A.B. would like to acknowledge the NAPLAS project, The Danish Council for Independent Research as well the European Research Council under the European Union's Seventh Framework Programme (FP7/2007-2013)/ERC grant agreement No. 320535. T.R. and A.B. also acknowledge financial support from the Danish National Research Foundation (DNRF122) and Villum Fonden (Grant No. 9301).

Competing interest: The authors declare no competing financial interest.

References

[1] Halas NJ, Lal S, Chang WS, Link S, Nordlander P. Plasmons in strongly coupled metallic nanostructures. Chem Rev 2011;111:3913–61.
[2] Willets KA, Van Duyne RP. Localized surface plasmon resonance spectroscopy and sensing. Annu Rev Phys Chem 2007;58:267–97.
[3] Anker JN, Hall WP, Lyandres O, Shah NC, Zhao J, Van Duyne RP. Biosensing with plasmonic nanostructures. Nature Mat 2008;7:442–53.
[4] Mayer KM, Hafner JH. Localized surface plasmon resonance sensors. Chem Rev 2011;111:3828–57.
[5] Talley CE, Jackson JB, Oubre C, Grady NK, Hollars CW, Lane SM, Huser TR, Nordlander P, Halas NJ. Surface-enhanced Raman scattering from individual Au nanoparticles and nanoparticle dimer substrates. Nano Lett 2005;5:1569–74.
[6] Pucci A, Neubrech F, Weber D, Hong S, Toury T, Lamy de la Chapelle M. Surface enhanced infrared spectroscopy using gold nanoantennas. Phys Status Solidi B 2010;247:2071–4.
[7] White JS, Veronis G, Yu Z, Barnard ES, Chandran A, Fan S, Brongersmal ML. Extraordinary optical absorption through subwavelength slits. Opt Lett 2009;34:686–8.
[8] Kim S, Jin J, Kim Y-J, Park I-Y, Kim Y, Kim S-W. High-harmonic generation by resonant plasmon field enhancment. Nature 2008;453:757–60.
[9] Valamanesh M, Borensztein Y, Langlois C, Lacaze E. Substrate effect on the plasmon resonance of supported flat silver nanoparticles. J Phys Chem C 2011;115:2914–22.
[10] Curry A, Nusz G, Chilkoti A, Wax A. Substrate effect on refractive index dependence of plasmon resonance for individual silver nanoparticles observed using darkfield micro-spectroscopy. Opt Express 2005;13:2668–77.
[11] Miller MM, Lazarides AA. Sensitivity of metal nanoparticle surface plasmon resonance to the dielectric environment. J Phys Chem B 2005;109:21556–65.
[12] Fernández-García R, Sonnefraud Y, Fernández-Domínguez AI, Giannini V, Maier SA. Design considerations for near-field enhancement in optical antennas. Contemp Phys 2014;55:1–11.
[13] Dmitriev A, Hägglund C, Chen S, et al. Enhanced nanoplasmonic optical sensors with reduced substrate effect. Nano Lett 2008;8:3893–8.
[14] Otte MA, Estévez M-C, Carrascosa LG, González-Guerrero AB, Lechuga LM, Sepúlveda B. Improved biosensing capability with novel suspended nanodisks. J Phys Chem C 2011;115:5344–51.
[15] Hatab NA, Hsueh C-H, Gaddis AL, Retterer ST, Li J-H, Eres G, Zhang Z, Gu B. Free-standing optical gold bowtie nanoantenna with variable gap size for enhanced Raman spectroscopy. Nano Lett 2010;10:4952–5.
[16] Caldwell JD, Glembocki O, Bezares FJ, et al. Plasmonic Nanopillar arrays for large-area, high-enhancement surface-enhanced Raman scattering sensors. ACS Nano 2011;5:4046–55.
[17] Cetin AE, Etezadi D, Altug H. Accessible nearfields by nanoantennas on nanopedestals for ultrasensitive vibrational spectroscopy. Adv Opt Mat 2014;2:866–72.
[18] Huck C, Toma A, Neubrech F, Chirumamilla M, Vogt J, De Angelis F, Pucci A. Gold nanoantennas on a pedestal for plasmonic enhancement in the infrared. ACS Photonics 2015;2:497–505.
[19] Chirumamilla M, Toma A, Gopalakrishnan A, et al. 3D nanostar dimers with a sub-10-nm gap for single-/few-molecule surface-enhanced Raman scattering. Adv Mater 2014;26:2353–8.
[20] Gopalakrishnan A, Chirumamilla M, De Angelis F, Toma A, Zaccaria RP, Krahne R. Bimetallic 3D nanostar dimers in ring cavities: recyclable and robust surface-enhanced Raman scattering substrates for signal detection from few molecules. ACS Nano 2014;8:7986–94.
[21] Li W-D, Ding F, Hu J, Chou SY. Three-dimensional cavity nanoantenna coupled plasmonic nanodots for ultrahigh and uniform surface-enhanced Raman scattering over large area. Opt Express 2011;19:3925–36.

[22] Zhang W, Ding F, Chou SY. Large enhancement of upconversion luminescence of $NaYF_4$: Yb^{3+}/Er^{3+} nanocrystal by 3D plasmonic nano-antennas. Adv Mater 2012;24:OP236–41.
[23] Shen Y, Zhou J, Liu T, et al. Plasmonic gold mushroom arrays with refractive index sensing figures of merit approaching the theoretical limit. Nat Comm 2013;4:1–9.
[24] Chen H, Bhuiya AM, Liu R, Wasserman DM, Toussaint Jr KC. Design, fabrication, and characterization of near-IR gold bowtie nanoantenna arrays. J Phys Chem C 2014;118:20553–8.
[25] Zou S, Schatz GC. Narrow plasmonic/photonic extinction and scattering line shapes for one and two dimensional silver nanoparticle arrays. J Chem Phys 2004;121:12606–12.
[26] Hicks EM, Zou S, Gunnarsson L, et al. Controlling plasmon line shapes through diffractive coupling in linear arrays of cylindrical nanoparticles fabricated by electron beam lithography. Nano Lett 2005;5:1065–70.
[27] Roxworthy BJ, Bhuiya AM, Yu X, Chow EKC, Toussaint Jr KC. Reconfigurable nanoantennas using electron-beam manipulation. Nat Comm 2014;5:1–7.
[28] Fu YH, Kuznetsov AI, Miroshnichenko AE, Yu YF, Luk'yanchuk B. Directional visible light scattering by silicon nanoparticles. Nat Comm 2013;1527:1–4.
[29] Gunnarson L, Rindzevicius T, Prikulis J, Kasemo B, Käll M. Confined plasmons in nanofabricated single silver pairs: experimental observations of strong interparticle interactions. J Phys Chem B 2005;109:1079–87.
[30] Johnson PB, Christy RW. Optical constants of the noble metals. Phys Rev B 1972;6:4370–9.
[31] Palik ED. Handbook of optical constants of solids. San Diego: Academic Press, 1998.
[32] Schmidt MS, Hubner J, Boisen A. Large area fabrication of leaning silicon nanopillars for surface enhanced Raman spectroscopy. Adv Mater 2012;24:OP11–8.
[33] Wu K, Rindzevicius T, Schmidt MS, Mogensen KB, Hakonen A, Boisen A. Wafer-scale leaning silver nanopillars for molecular detection at ultra-low concentrations. J Phys Chem C 2015;119:2053–62.
[34] Shegai T, Brian B, Miljković VD, Käll M. Angular distribution of surface-enhanced Raman scattering from individual AU nanoparticle aggregates. ACS Nano 2011;5:2036–41.

Supplemental Material: The online version of this article (DOI: 10.1515/nanoph-2017-0011) offers supplementary material, available to authorized users.